Electrical Engineering & Computer Science
Faculty Publications

Electrical Engineering & Computer Science
Department

11-2018

Active Disturbance Rejection Control of LCL-Filtered Grid-Connected Inverter Using Pade Approximation

Abdeldjabar Benrabah
Harbin Institute of Technology

Dianguo Xu
Harbin Institute of Technology

Zhiqiang Gao
Cleveland State University, Z.GAO@csuohio.edu

Active Disturbance Rejection Control of *LCL*-Filtered Grid-Connected Inverter Using Padé Approximation

Abdeldjabar Benrabah ⓘ, Dianguo Xu ⓘ, *Fellow, IEEE*, and Zhiqiang Gao ⓘ, *Member, IEEE*

Abstract—In this paper, a simplified robust control is proposed to improve the performance of a three-phase current controlled voltage source inverter connected to the grid through an inductive–capacitive–inductive (*LCL*) filter. The presence of the *LCL*-filter resonance complicates the dynamics of the control system and limits its overall performance, particularly when disturbances and parametric uncertainty are considered. To solve this problem, a robust active damping method based on the linear active disturbance rejection control (LADRC) is proposed. The simplification is made possible by order reduction in the plant transfer function using Padé approximation. Simulation results show that the proposed LADRC-based current controller achieves high power quality and good dynamic performance, in the presence of parameters uncertainties as well as external disturbances. An experimental prototype is built to verify the effectiveness and practicality of the proposed control strategy.

Index Terms—Active damping, active disturbance rejection control (ADRC), grid-connected inverter, *LCL* filter, Padé approximation.

I. INTRODUCTION

VOLTAGE source inverter (VSI) exhibits several features that make it attractive in many power conversion applications particularly in renewable energy and distributed generation systems as an interface converter between the utility grid and the power sources [1], [2]. The inductive–capacitive–inductive (*LCL*) filters are commonly used at the inverter ac terminals in order to reduce the switch ripples and improve the power quality to meet the grid-connection standard requirements. However, the current control of the *LCL*-filter-based grid-connected VSI is a challenging issue due to the underdamping characteristics of the *LCL* filter caused by the resonance that needs to be passively or actively damped [3].

Passive damping can be simply implemented by adding a resistor in series with the filter capacitor but leads to additional power losses and degradation of the filter attenuation performance [4]. Active damping methods damp the *LCL*-filter resonance through a modification in the current control loop without using dissipative components, by feeding back one of the filter state variables [5], [6] or by adding a digital filter in cascade with the current controller [7]. However, such kinds of controllers may fail to meet the high-performance requirements of grid-connected applications due to their high vulnerability to parameters variation and disturbances.

In order to improve the stability performance of the *LCL*-filtered grid-connected inverters, many robust active damping controls have been proposed. A self-commissioning notch-filter-based active damping control was proposed by continuously estimating the resonant frequency and adjusting the notch filter accordingly but this method inevitably increases the computational burden when implemented in digital controllers [8]. Massing *et al.* [9] proposed an adaptive state feedback controller with a more complex algorithm and several gains to be tuned to ensure stability under grid impedance variation and grid disturbance. A robust feedback-type control with reduced computation delay is developed in [10] but additional sensor is needed for its implementation. In [11], additional capacitor voltage sensor is used to damp the filter resonance and an adaptive estimator is used to deal with grid disturbance and parametric instabilities. A cost-effective deadbeat controller with an adaptive predictor is proposed in [12] to deal with grid inductance variation and grid voltage distortion but its stability is not guaranteed due to the model-based nature of the proposed controller. Another disturbance estimator is proposed in [13] by using uncertainty and disturbance estimator for robust current control but additional sensor is required for active damping.

In the last few years, an emerging control technology known as active disturbance rejection control (ADRC), has been explored in almost all domains of control engineering as an alternative option to the conventional PID controllers and modern model-based control strategies [14], [15]. In order to simplify the structure of the ADRC, Gao used linear gains to replace the nonlinear gains in the control algorithm [16], and which is linear active disturbance rejection control (LADRC). Unlike many existing control methods, the ADRC does not require the accurate mathematical model of the plant [17]. Moreover, selecting the plant order n (or the relative degree) of the ADRC is quite flexible, which makes this control more convenient to apply in many control systems [18]–[20]. In this paper, based on a low-order
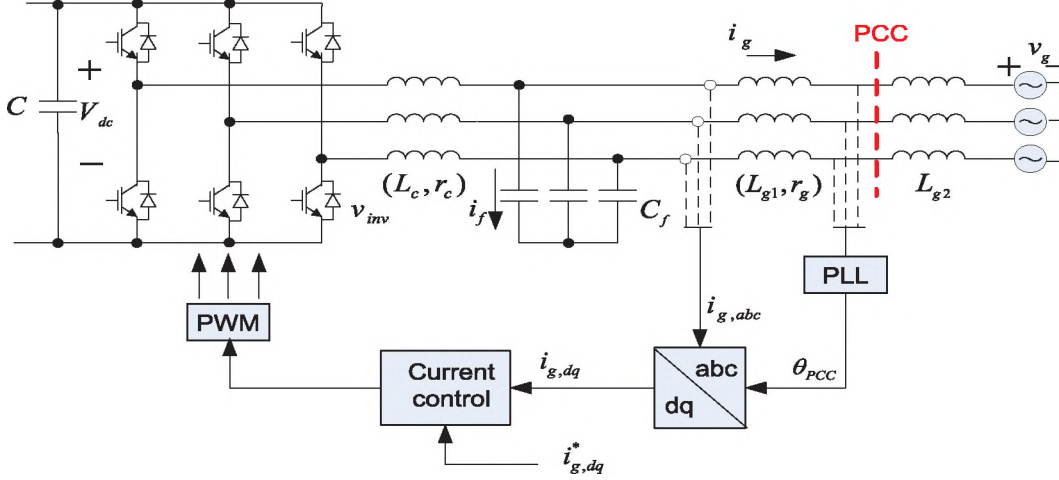
Fig. 1. *LCL*-filter-based three-phase grid-connected inverter.

Parameters	Symbols	Value
Converter side inductance	L_c	6 mH
Grid side inductance	L_g	3 mH
Filter capacitor	C_f	10 μF
DC link voltage	V_{dc}	480V
Grid voltage	v_g	110V
Frequency of the grid voltage	f	50 Hz
Switching/Sampling frequency	f_{sw}	10 kHz
Nominal power	P	1.1 kW

approximation, the first-order linear ADRC controller is applied to the *LCL*-filtered grid-connected VSIs to deal with parameters variation and disturbances, which will greatly simplify the control design of the control method presented in [21].

The remainder of this paper is structured as follows. Section II reveals the stability problems of the *LCL*-filter-based grid-connected VSI. In Section III, a simplified ADRC-based control design is proposed by using Padé approximation to reduce the model order of the system. The feasibility and validity of the proposed control method are verified both by numerical simulations and experimentally on laboratory prototype in Sections IV and V, respectively. Finally, conclusions are drawn in Section VI.

II. STABILITY PROBLEM OF THE *LCL*-FILTER-BASED GRID-CONNECTED VSI

The block diagram of the current-controlled grid-connected VSI in the *dq* synchronous reference frame (SRF) is shown in Fig. 1. A third-order *LCL* filter is used at the terminal of the inverter in order to attenuate the switching harmonics injected into the grid. The power system parameters used in the study of this paper are listed in Table I. The design procedure of the *LCL*

filter is described in [2]. The reference frequency and phase of the grid voltage at the point of common coupling are provided by a phase-locked loop to perform the *dq* transformation. The active and reactive power exchanged with the grid are determined by the *d*-axis current reference i_d^* and the *q*-axis current reference i_q^*, respectively. Assuming that a dc power supply is used to power the voltage source converter in Fig. 1, therefore, no controller is required to regulate the dc-link voltage (otherwise, another controller is needed to regulate the dc-link voltage and generate the *d*-axis current reference accordingly).

Modeling the *LCL* filters in the *dq* SRF gives

$$L_g \frac{di_g^{dq}}{dt} = v_g^{dq} - v_C^{dq} - (r_g + j\omega L_g)i_g^{dq}$$

$$C_f \frac{dv_C^{dq}}{dt} = i_g^{dq} - i_C^{dq} - j\omega C_f v_C^{dq}$$

$$L_c \frac{di_{inv}^{dq}}{dt} = v_C^{dq} - v_{inv}^{dq} - (r_c + j\omega L_c)i_c^{dq} \qquad (1)$$

where $L_g = L_{g1} + L_{g2}$, r_c, and r_g are the equivalents series resistances of the converter- and grid-side inductances.

The Bode plot of the transfer function consistent with (1) is shown in Fig. 2. A sharp resonance peak is noticeable at the resonance frequency that can be passively or actively damped. Passive damping methods involve additional power loss and reduce the overall system efficiency; therefore, active damping methods are highly recommended.

In practice, the filter parameters may vary as a consequence of variable operating conditions and component aging effects. In addition, the grid inductance at the point of connection can be considered as a part of the grid-side filter inductance; thus, the grid inductance uncertainty may result in changes in the *LCL*-filter resonance frequency, which challenges the current controller design. The effect of parameters variation on system stability is more obvious when using active damping methods. Cascading a digital filter in series with the reference voltage modulator, for example, which is often used to attenuate the open-loop gain at the resonant frequency by tuning the notch
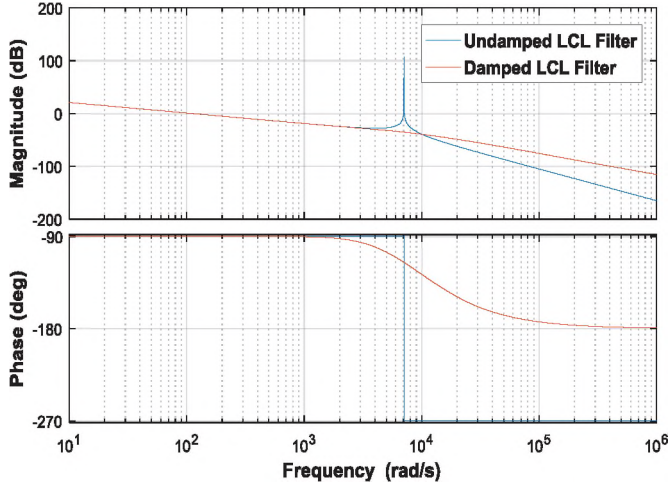
Fig. 2. Bode plot of undamped and passively damped *LCL* filter.

Fig. 3. Control scheme of first-order linear ADRC.

frequency at the resonance frequency, is directly affected by small variations of the grid inductance [8].

Another challenge that compromises the stability of the current controller is the presence of the grid disturbances [1], [22], [23]. Investigations in [1] showed that a small level in grid voltage harmonic distortion increases significantly the total harmonic distortion (THD) of the injected current and eventually may lead to system instability due to possible interactions between the grid disturbances and the distributed generation interface. Therefore, high rejection capability of grid disturbances is one of the important properties that should be considered in the current controller of grid-connected applications.

III. PROPOSED LADRC-BASED ROBUST CONTROL DESIGN

It can be concluded from the above-mentioned control viewpoints that robustness against parameters variation and disturbances must be a key attribute in the *LCL*-filtered grid-connected inverter control to guarantee the system stability. This paper proposes the application of the ADRC to ensure good tracking of the current reference, good attenuation of the *LCL*-filter resonance, and robust stability with respect to parametric variations and disturbances.

A. Brief Summary of ADRC

Consider the following nth-order plant with single-input, u, and single-output, y

$$y^{(n)}(t) = f(y^{(n-1)}, y^{(n-1)}, \ldots, y(t), w(t)) + bu(t) \quad (2)$$

where w is the internal disturbances including the unmodeled dynamics and parameters uncertainties, and b is a given constant. $f(y^{(n-1)}, y^{(n-2)}, \ldots, y^{(n)}, w(t))$, or simply f, represents the overall dynamics of the plant that is unknown. Hence, for this plant, the accurate model is not available. The ADRC is a
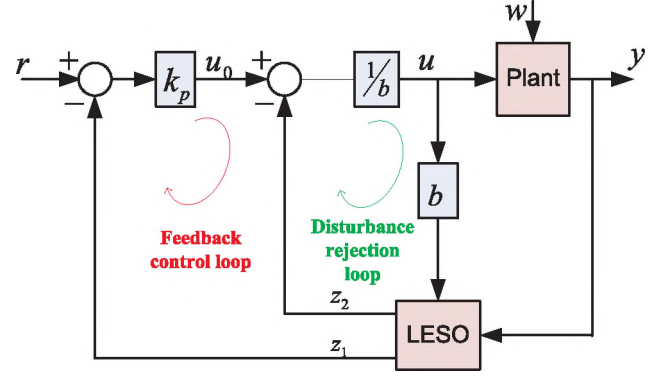
unique method designed to tackle this kind of problem. Unlike traditional control approach based on explicit modeling of the plant, the ADRC is an alternative that impressively reduces the dependence on the system model.

The tuning procedure of the ADRC was greatly simplified by Gao based on the concept of bandwidth, and the number of parameters was also reduced by using the linear gains in place of the original nonlinear gains [16]. Many studies showed that the LADRC still achieved high performance and good robustness [16], [24].

The structure of the first-order ADRC is shown in Fig. 3. It consists of two main control loops. The inner loop, also referred to as the disturbance rejection loop, is responsible for compensating the total disturbance. The effectiveness of this control loop is governed by an accurate estimation of the total disturbance by the linear extended state observer (LESO). The outer loop, also referred to as the feedback control loop, is responsible for realization of the desired signal by using a feedback controller.

B. Problem Formulation

Using a three-order *LCL* filter is a challenging issue in the current controller design. In fact, the simplification of high-order transfer functions by low-order models is often helpful in the analysis and design of control systems, and a low-order ADRC controller is usually preferred in practice. Approximating the *LCL* filter with a first-order system (same order as an *L* filter) for control design can be achieved by using Padé approximation as proposed in [25]. The Padé approximant $P_{N,M}(x)$ of a function $f(x)$ is defined as the ratio of two polynomials, with degrees N and M, having the same Taylor series expansion up to degree $M + N$ [26]. Considering the *LCL*-filter transfer function from the inverter output voltage v_{inv} to the injected grid current i_g when the grid voltage is neglected written as follows:

Pena-Alzola *et al.* [25] showed that the first-order Padé approximant $P_{0,1}(x)$ of (3), shown at the bottom of the page, can

$$H_{LCL}(s) = \frac{i_g}{v_{inv}} = \frac{1}{L_c L_g C_f s^3 + (r_c L_g C_f + r_g L_c C_f)s^2 + (L_c + L_g + r_c r_g C_f)s + r_c + r_g} \quad (3)$$
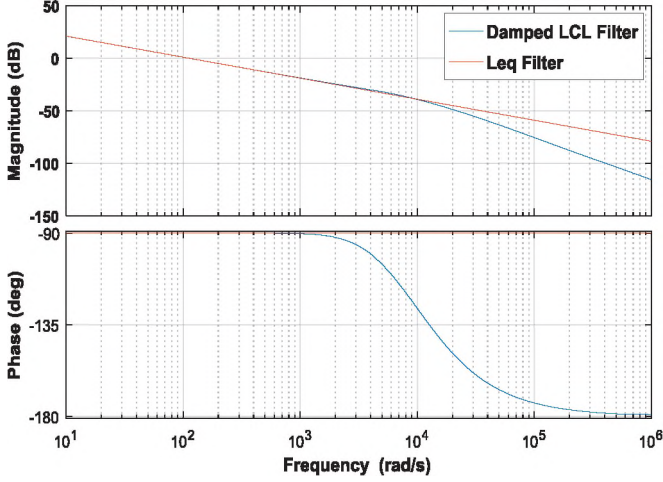
Fig. 4. Bode plot of the LCL filter and equivalent L_{eq} filter.

be used as an equivalent model for control design in the dq reference frame. The Padé approximant $P_{0,1}(x)$ is given by

$$H_{\text{Pade}}(s) = \left(\frac{i_g}{v_{\text{inv}}}\right)_{\text{Pade}} = \frac{1}{(L_c + L_g + r_c r_g C_f)s + r_c + r_g}.$$

(4)

This is almost the same as the transfer function of the L filter corresponding to the sum of inductances of the LCL filter $(L_c + L_g) + r_c + r_g$, since the additional terms are very small.

This approximation can be explained by the fact that in the low-frequency range, the filter capacitor can be neglected and the LCL filter behaves like an equivalent inductor $L_{\text{eq}} = L_g + L_c$ including the equivalent series resistances $r_{\text{eq}} = r_g + r_c$. However, this approximation is unfortunately true only when considering the magnitude response. As shown in Fig. 4, over the low-frequency range, an optimally damped LCL filter has the same magnitude as an equivalent inductor L_{eq}, but their phases are quite different. In [27], it is suggested to choose the crossover frequency as a fraction of the resonance frequency ($\omega_c = \alpha.\omega_{\text{res}}$). When the LCL filter is optimally damped, the crossover frequency is computed such as $\alpha = 0.3$. In this way, the phase lag introduced by the LCL filter is about $115°$, which is not very severe degradation compared with that of the L filter ($90°$).

In the ADRC framework, the approximation error between the considered system and the real system and other disturbances including the resonance, all of which are seen as disturbance and are actively compensated [28]. The control design is then done with the equivalent inductor approximation of the LCL filter. Even if this approximation is not suitable for the high-frequency range, it has been intentionally kept to reduce the system order for the ADRC design. Making the assumption that the precise mathematical model of the system is unknown and considering the external disturbance w, the system dynamics of the LCL filter based on the approximated model can be reformulated in the ADRC framework as follows:

$$\dot{y} = f(t, y, w) + bu$$

(5)

where $f(\cdot)$ represents the "total disturbance" to be estimated and mitigated including both external disturbances and internal dynamics, y represents the grid current, u is the control input applied to the inverter, and b is a system parameter.

For the first-order reduced model, the output y is defined as the first state x_1 as usual; additionally, the total disturbance f is defined as the extended state x_2. Assuming that f is differentiable, the system dynamics (5) can be defined in the state space form for the augmented vector state x as follows:

$$\begin{cases} \dot{x}(t) = Ax(t) + Bu(t) + E\dot{f}(t) \\ y(t) = Cx(t) \end{cases}$$

(6)

where

$$A = \begin{bmatrix} 0 & 1 \\ 0 & 0 \end{bmatrix}, B = \begin{bmatrix} b \\ 0 \end{bmatrix}, E = \begin{bmatrix} 0 \\ 1 \end{bmatrix}, C = \begin{bmatrix} 1 & 0 \end{bmatrix}.$$

The corresponding second-order LESO built over the reduced model is then written as follows:

$$\begin{cases} \dot{z}(t) = Az(t) + Bu(t - T_d) + L(y(t) - \hat{y}(t)) \\ \hat{y}(t) = Cz(t) \end{cases}$$

(7)

where $L = [\beta_1 \ \beta_2]^T$ is the observer gain vector. The observer gains are selected such that all the observer eigenvalues are placed at $-\omega_o$, and they are found to be $\beta_1 = 2\omega_o$, $\beta_2 = \omega_o^2$. With appropriate selection of β_1 and β_2, the observer states z_1 and z_2 will track y and f, respectively.

Compared with the regular ADRC control, the control input u is delayed before it goes into the LESO to take account of the time delay T_d as proposed in [29]. This modification will synchronize the observer inputs and allow it to provide meaningful estimations of the delayed system states and delayed disturbances since the system output is already delayed due to the system dynamics. Although the modification is simple, it improves the regular ADRC control by increasing the observer bandwidth, which is the key for an accurate estimation of total disturbance [14], [29].

Finally, the total disturbance is compensated in the disturbance rejection loop by applying

$$u = \frac{u_0 - \hat{f}}{b}$$

(8)

where u_0 is the amount of control before compensation and the estimate of f is the estimated total disturbance denoted by z_2.

So that (5) becomes

$$\dot{y} = f + bu = f - \hat{f} + u_0 \approx u_0$$

(9)

forcing the plant to behave as a pure integrator, which can be easily controlled using a linear proportional controller of the form

$$u_0(t) = k_p(r(t) - z_1(t))$$

(10)

where r is the desired reference input (see Fig. 3) and k_p is the controller gain.

Substituting (10) into (9) results in

$$\dot{y} + k_p y = k_p r.$$

(11)

Then, the transfer function of the closed-loop control system when the disturbance is compensated is given by

$$G_{ry}(s) = \frac{y(s)}{r(s)} = \frac{k_p}{s + k_p}. \qquad (12)$$

C. Stability Analysis

To investigate the system stability and the performance using the frequency response, some simplifications are done in the s-domain. By applying Laplace transform to (7), we can obtain

$$z_1 = \frac{\beta_1 sy + k_p sr}{s(s + \beta_1 + k_p)} \qquad (13)$$

$$z_2 = \frac{\beta_2 s + \beta_2 k_p y - \beta_2 k_p r}{s(s + \beta_1 + k_p)}. \qquad (14)$$

By combining (8), (10), (13), and (14), the ADRC-based control law can be expressed as

$$u(s) = G_c(s)(r(s) - H(s)y(s)) \qquad (15)$$

where

$$G_c(s) = \frac{1}{b} \frac{k_p(s^2 + \beta_1 s + \beta_2)}{s(s + \beta_1 + k_p)} \qquad (16)$$

$$H(s) = \frac{(k_p \beta_1 + \beta_2)s + \beta_2 k_p}{k_p(s^2 + \beta_1 s + \beta_2)}. \qquad (17)$$

Finally, by substituting (15) into (5) in the s-domain, the control output is derived as follows:

$$\begin{aligned}
y(s) &= \frac{1}{s}(f(s) + bu(s)) \\
&= \frac{1}{s}(f(s) + bG_c(s)(r(s) - H(s)y(s))) \\
&= \frac{(s + \beta_1 + k_p)}{(s + k_p)(s^2 + \beta_1 s + \beta_2)}sf(s) + \frac{k_p}{s + k_p}r(s) \\
&= G_{fy}(s)f(s) + G_{ry}(s)r(s). \qquad (18)
\end{aligned}$$

Obviously, the stability of the closed-loop control depends only on the control bandwidth and the observer bandwidth [30]. According to (18), the control output consists of the reference tracking term and disturbance rejection term. If the disturbance $f(s)$ is neglected, the output is simplified as (12). In this case, the tracking performance depends on the control bandwidth $k_p = -\omega_c$. Fig. 5 shows that by increasing the control bandwidth, the stability margin is more expanded and the tracking speed is faster. The high-pass filtering is also improved as the high-frequency gains increase.

When considering the disturbance rejection term, we can see that the disturbance rejection is decided by the bandwidths of the controller and the observer. The frequency responses in Figs. 6 and 7 show that increasing the observer bandwidth or the control bandwidth yields better disturbance rejection performance. In practice, the observer bandwidth is usually chosen seeking a compromise between the speed of states estimation and noise sensitivity while the control bandwidth is chosen according to a desired settling time.
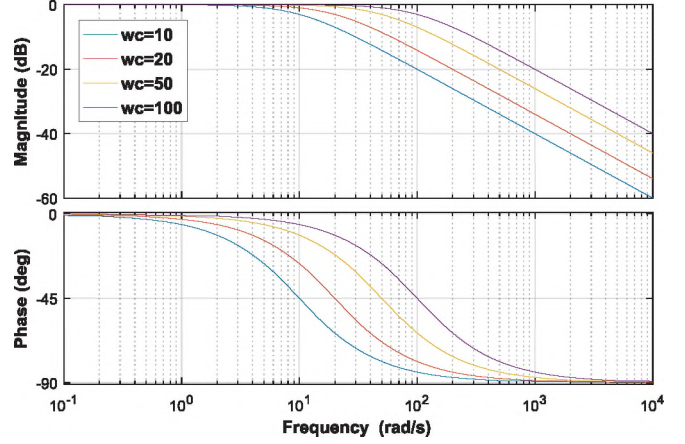

Fig. 5.   Bode plot of $G_{ry}(s)$ by changing the control bandwidth ω_c.
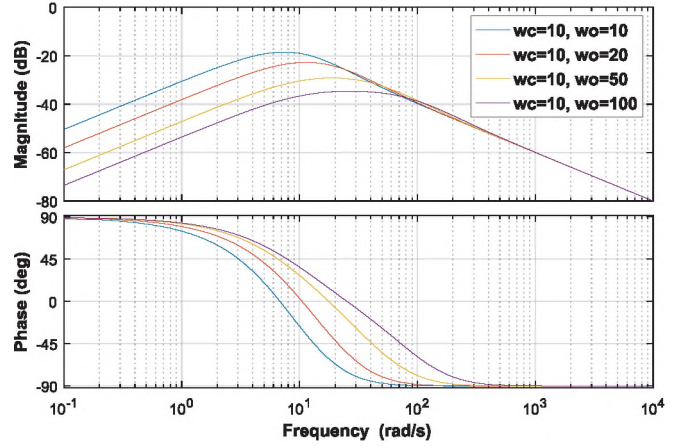

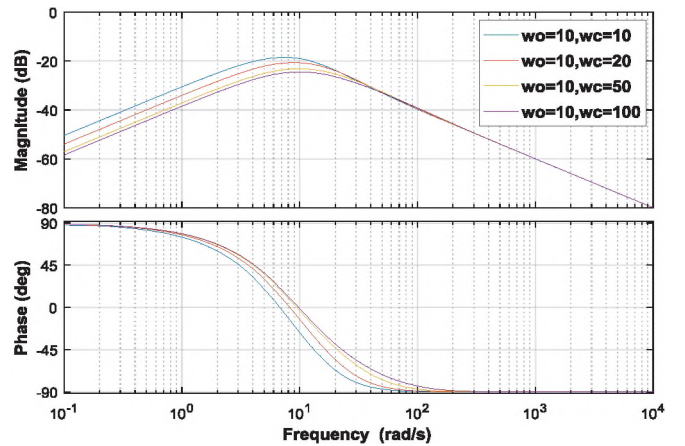Fig. 6.   Bode plot of $G_{fy}(s)$ by changing the observer bandwidth ω_o.

Fig. 7.   Bode plot of $G_{fy}(s)$ by changing the control bandwidth ω_c.

D. Control Design

For the control design, one needs to choose k_p, β_1, β_2, and the value of b. The controller gain k_p is obtained by locating the closed-loop pole according to a desired settling time T_{settle}.

From (12), we can obtain

$$k_p = -\omega_c, \text{ with } \omega_c \approx -\frac{4}{T_{\text{settle}}}. \qquad (19)$$

The observer gains are selected such that all the observer eigenvalues are placed at $-\omega_o$ such as $\omega_o \approx 3\text{--}10\omega_c$, and they are found to be

$$\beta_1 = 2\omega_o, \quad \beta_2 = \omega_o^2. \qquad (20)$$

In this way, the LESO is simply characterized by the observer bandwidth ω_o [16]. The observer bandwidth is usually chosen seeking a compromise between the speed of states estimation and noise sensitivity.

Finally, the value of b should be increased gradually to the corresponding value that satisfies the dynamic performance.

For a discrete-time implementation [31], the continuous plant model in (6) can be expressed in the discrete form as follows:

$$\begin{cases} x(k+1) = A_d x(k) + B_d u(k) \\ y(k) = C_d x(k) \end{cases} \qquad (21)$$

where

$$A_d = I + \sum_{i=1}^{\infty} \frac{A^i . T_{\text{sample}}^i}{i!} = \begin{bmatrix} 1 & T_{\text{sample}} \\ 0 & 1 \end{bmatrix}$$

$$B_d = \left(\sum_{i=1}^{\infty} \frac{A^{i-1} . T_{\text{sample}}^i}{i!} \right) B = \begin{bmatrix} b T_{\text{sample}} \\ 0 \end{bmatrix}$$

$$C_d = C. \qquad (22)$$

The LESO in (7) can also be written in the discrete form as follows:

$$\begin{cases} z(k+1) = A_d z(k) + B_d u(k - \tau(k)) + L_d(y(k) - \hat{y}(k)) \\ \hat{y}(k) = C z(k) \end{cases}$$
$$\qquad (23)$$

where the integer $\tau(k) > 0$ denotes the amount of time delay. The desired observer poles have to be located to the z-domain via

$$\omega_{od} = e^{-\omega_o . T_{\text{Sample}}}. \qquad (24)$$

Then, the discrete observer gains can be calculated by

$$\beta_1 = 1 - \omega_{od}^2, \quad \beta_2 = \frac{(1 - \omega_{od})^2}{T_{\text{sample}}}. \qquad (25)$$

The control law in (10) is expressed in the discrete form only by exchanging time t with the current sample point k

$$u(k) = k_p(r(k) - z_1(k)). \qquad (26)$$

The overall controller diagram of the three-phase LCL-filtered grid-tied system in the dq reference frame is shown in Fig. 8(a). One independent first-order LADRC controller is designed for each current component (i.e., d-axis and q-axis current). The reference voltage is delayed before it goes into LESO by adding a time delay block T_d as proposed in [29]. Compare with the classical PI-based control shown in Fig. 8(b), the cross-coupling terms and the feed-forward grid voltage are considered as an
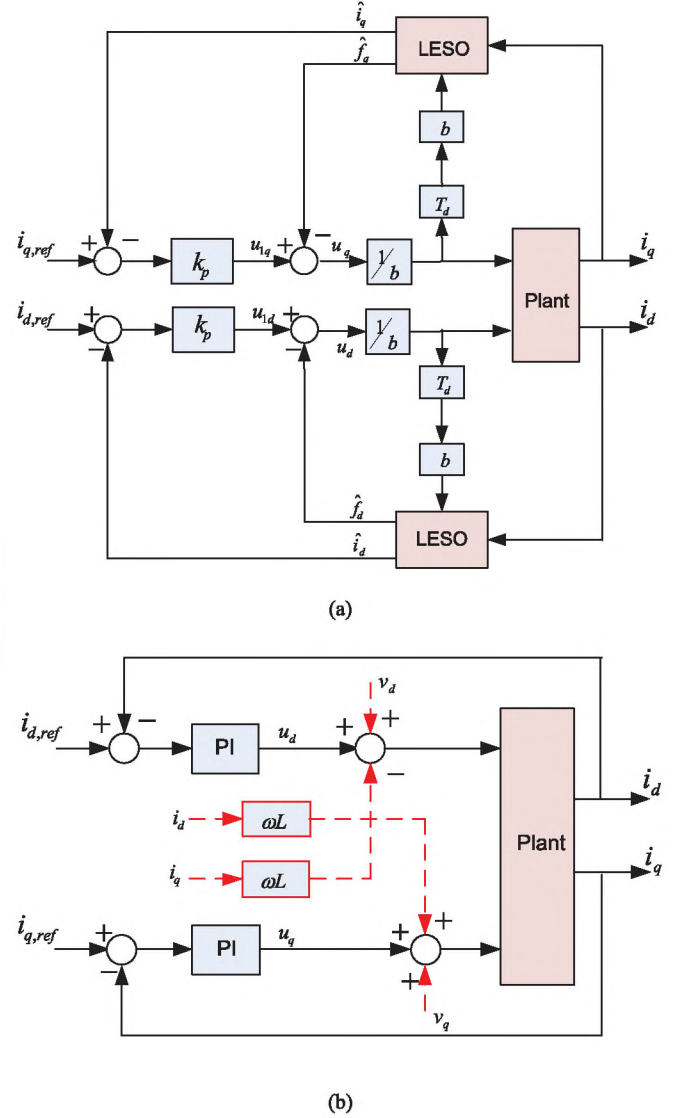
external disturbance in the ADRC [32]–[34]. Therefore, the same parameters can be used for the d- and q-current controllers. Moreover, the LCL-filter resonance is estimated and mitigated in the compensation control loop without additional sensor or adaptive control in contrast to the PI-based control where an active damping control should be added to ensure the system stability. The designed controller parameters are listed in Table II.
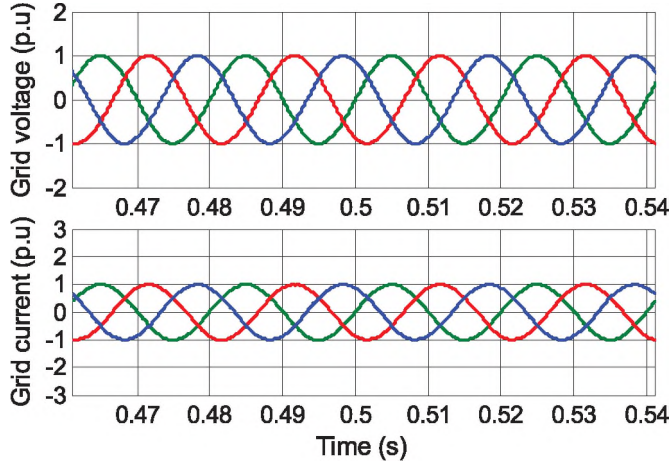

Fig. 8. Current control scheme of the LCL-filtered grid-connected inverter. (a) Proposed ADRC-based control. (b) PI-based control.

TABLE II
CONTROLLER PARAMETERS

Parameters	Symbols	Value
Controller gain	k_p	30
Observer bandwidth	ω_o	90
Compensation factor	b	125

Fig. 9. Grid voltage and grid current responses under nominal power operation.
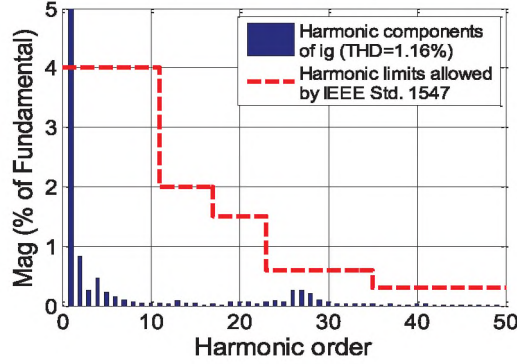

Fig. 10. Harmonic components of i_g respecting limits allowed by IEEE Std. 1547 and with a THD of 1.16%.

IV. PERFORMANCE EVALUATION RESULTS

To evaluate the performance of the proposed LADRC-based active damping method with the designed controller parameters determined in the previous section, simulations have been carried out in the MATLAB/Simulink environment based on the system shown in Fig. 1 and the current controller shown in Fig. 4(a). The power system and the controller parameters are listed in Tables I and II, respectively.

A. Steady-State Performance and Resonance Damping

The simulation results of the proposed ADRC-based active damping method under nominal power operation are shown in Figs. 9 and 10. The grid current is regulated to its nominal value and is in phase with the grid voltage as can be seen in Fig. 9. The steady-state harmonic analysis of the grid current comply with harmonic and THD requirements from the IEEE Standard 1547, as shown in Fig. 10, confirming the good quality of the current injected into the grid. The high-quality current injection is the natural result of the effective damping of the resonance and the high disturbance rejection ability of the proposed current controller.
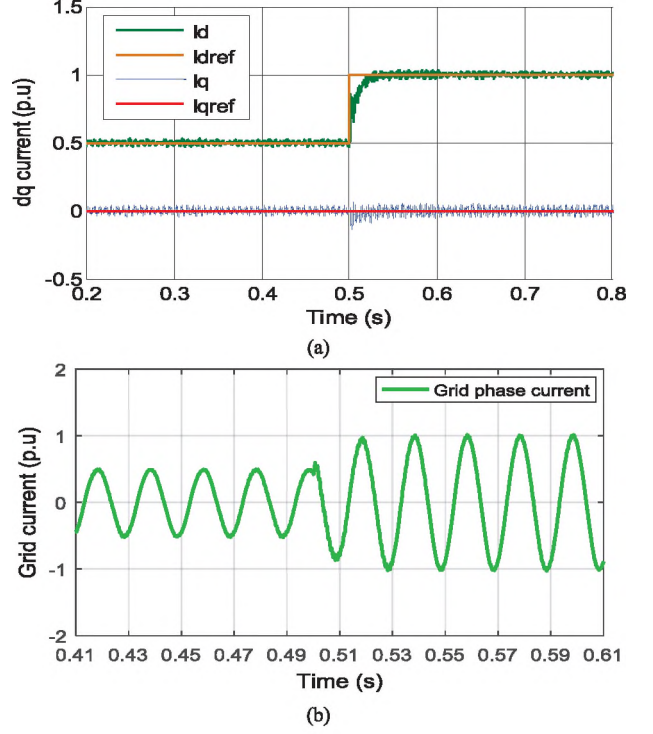

Fig. 11. Simulation results of the grid current response when the d-axis grid current reference changes from 0.5 to 1 p.u. using the ADRC control method. (a) Transient responses of the dq-axis components of grid current. (b) Transient responses of the grid-phase current.

B. Transient Response and Decoupling Effectiveness

The grid current transient responses using the proposed ADRC controller for stepping up the grid current reference from 0.5 to 1.0 p.u. and then for stepping down the grid current reference from 1.0 to 0.5 p.u. are shown in Figs. 11 and 12, respectively. For simplicity, results of only phase-A in p.u. values are shown in Figs. 11(a) and 12(a). The dq-axis current are also depicted in Figs. 11(b) and 12(b). As can be seen, the proposed control strategy is capable of tracking the grid current change, so that the active and the reactive power can be controlled independently. The coupling term effect between the d- and q-components is virtually nonexistent. Furthermore, the proposed ADRC control provides better dynamic performance without overshoot and with fast transient response.

C. Robustness Under Parameter Variations

The effectiveness of the ADRC-based active damping control under parameter variations is compared with the notch-filter-based active damping control. Simulation results of the grid current waveforms are shown in Fig. 13. As shown in Fig. 13(a), the oscillations in the grid current can be noticed without active damping due to the LCL-filer resonance. When the active damping is enabled, the system becomes stable after a short transient as the notch filter is perfectly tuned on the resonance frequency. When the grid inductance is increased from 100% to 150% of the nominal inductance at 0.3 s, the system loses again its stability due to inadequate damping of
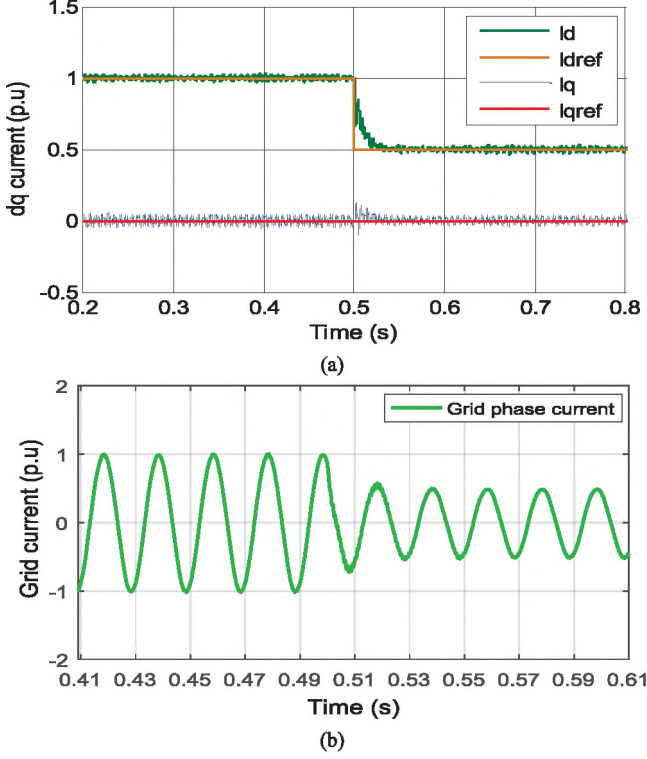
Fig. 12. Simulation results of the grid current response when the d-axis grid current reference changes from 1 to 0.5 p.u. using the ADRC control method. (a) Transient responses of the dq-axis components of grid current. (b) Transient responses of the grid-phase current.
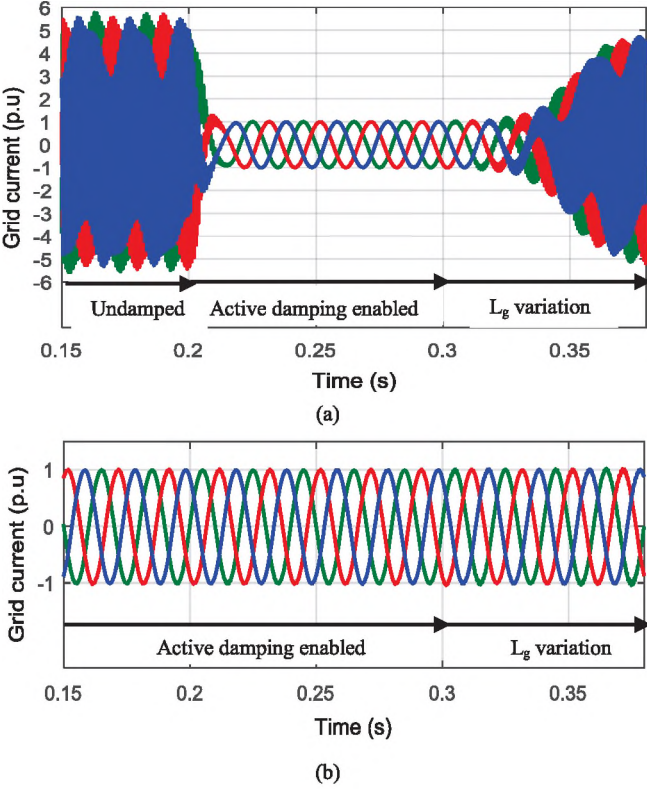

Fig. 13. Three-phase grid current response under grid inductance variation. (a) Filter-based active damping control. (b) ADRC-based active damping control.
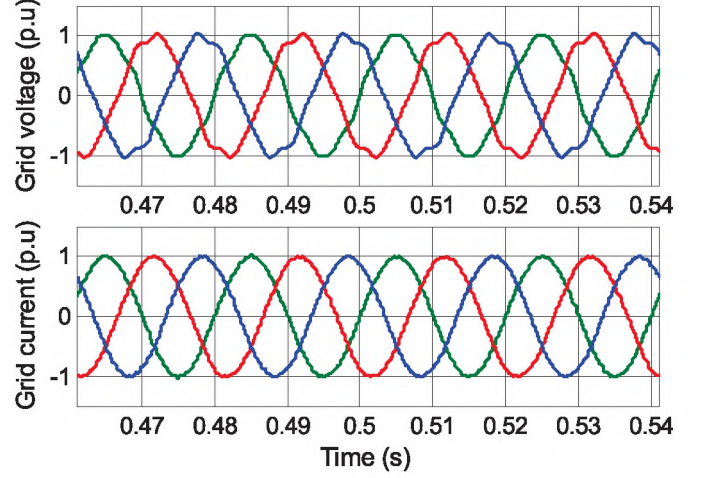

Fig. 14. Grid voltage and grid current responses under grid voltage disturbances (THD = 1.95%).

the *LCL*-filter resonance. The notch filter cannot keep the resonance damped as the resonance frequency varies too much. The undesirable effect of the parameters variation can be mitigated by the ADRC as shown in Fig. 13(b). The proposed method effectively suppresses the *LCL*-filter resonance even after sudden variation of the resonance frequency, providing a stable system performance before and after parameter variation, which means that the proposed control has the inherent advantage of excellent adaptability for operation environment. Thus, the ADRC control offers a superior feature in comparison with filter-based active damping control. It is worth noting that the failure of the notch-filter-based active damping control remains of interests for developing other solutions to deal with grid inductance variations, for example, by continuously estimating the resonant frequency and adjusting the notch filter accordingly. However, this solution needs an online estimation, which will inevitably increase the control design complexity [8]. That is to say that the lower complexity of the notch-filter-based control may come at the price of lower effectiveness. On the other hand, the proposed method with a minimum complexity in the controller design and without any adaptive algorithm, still ensure the system stability under parameter variations.

D. Robustness Under Grid Uncertainties and Disturbances

The controller is evaluated at uncertain grid conditions with 150% L_g and with the following grid distortion levels: 5% fifth harmonic and 3% seventh harmonic. Fig. 14 shows the high quality of the current injected to the grid with the proposed current control scheme with a THD of 1.95%. This result meets the grid-connection standards requirements. The grid voltage harmonic disturbances are rejected by the robust ADRC controller, leading to a much better performance.

V. EXPERIMENTAL RESULTS

A laboratory prototype has been built to experimentally validate the effectiveness of the proposed control method. The
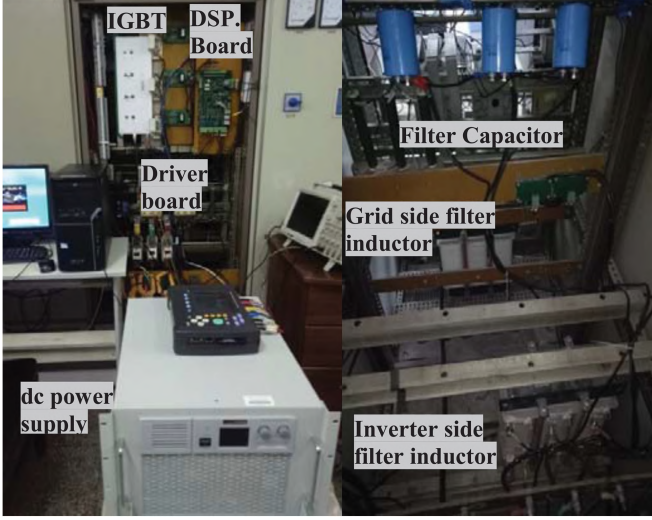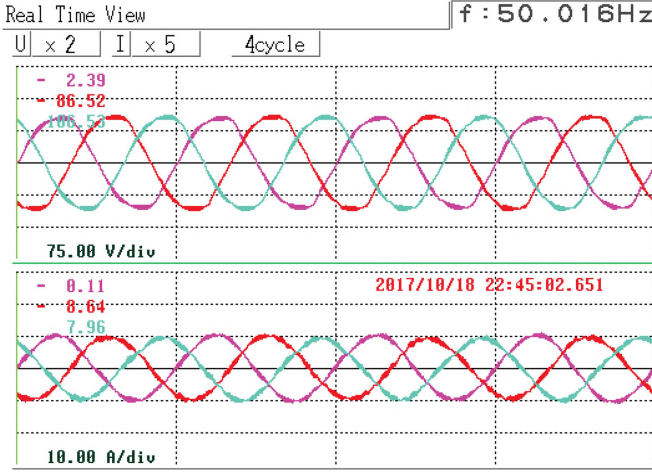
Fig. 15. Photograph of the experimental setup.

Fig. 16. Experimental steady-state waveforms of grid-phase voltages and grid-phase currents, waveforms obtained using power quality analyzer HIOKI 3196.

control system used in simulations has been implemented by using a 32-b floating-point digital signal controller DSP TMS320F28335 from Texas Instruments with a sampling frequency of 10 kHz. Fig. 15 shows a photograph of the experimental setup that includes the following: ac power source, voltage regulating transformer, DSP control board, three-phase PWM VSI with the *LCL* filter, dc power supply, digital phosphor oscilloscope Tektronix DPO4104, and a power quality analyzer HIOKI 3196. The designed system and controller parameters are the same as those used for simulation. The robustness of the proposed ADRC controller under parameter variations has been verified experimentally for different values of the grid-side filter inductor then compared with the well-known notch-filter-based active damping control.

A. Steady-State Response

The performances of the ADRC control have been verified by implementing different experimental tests. The first test is

Fig. 17. Experimental results for the values of THD and PF for each phase, obtained using power quality analyzer HIOKI 3196.
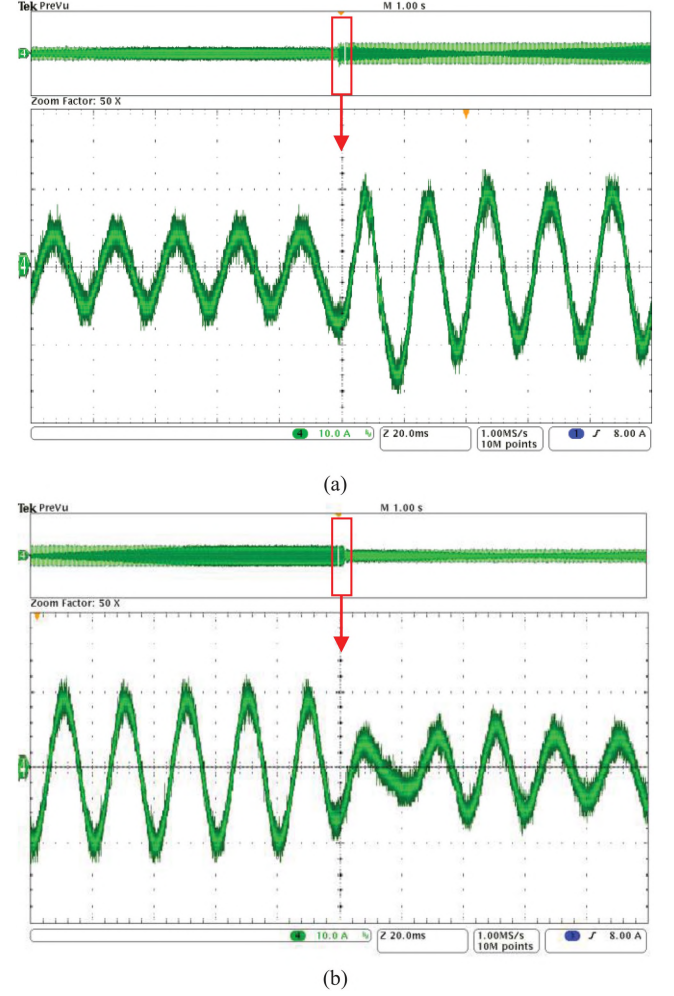

(a)

(b)

Fig. 18. Grid-phase current i_{ga} for a step changes in the d-axis reference amplitude, waveforms obtained using digital phosphor oscilloscope Tektronix DPO4104. (a) Experimental step-up response of the grid-phase current i_{ga} (10 A/div). (b) Experimental step-down response of the grid-phase current i_{ga} (10 A/div).

oriented to verify the steady-state performance under nominal power operation with a reference current equal to $i_{ref} = 10$ A. As can be seen in Fig. 16, the proposed ADRC control provides notable performance since the grid current tracks the reference current perfectly and the *LCL*-filter resonance is actively damped. The THD value of each phase current is below 3%, which meets the specified harmonic standards in industrial applications as can be seen in Fig. 17. Moreover, the reactive power is almost kept zero, meaning a quasi-totality injection of the energy as active power into the grid, and a near unity power factor (PF) is achieved since the grid voltage and current are kept in phase.
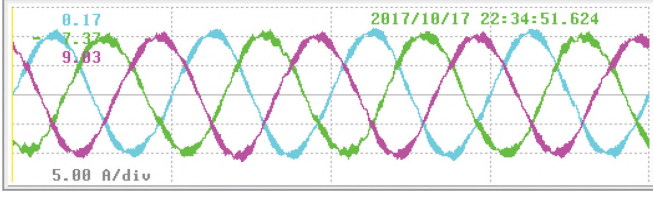
Fig. 19. Stable performance of the ADRC-based active damping control under grid-inductance variation. Waveforms obtained using the power quality analyzer HIOKI 3196.
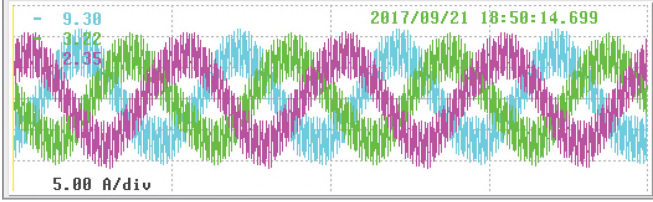

Fig. 20. Unstable performance of the filter-based active damping under grid-inductance variation. Waveforms obtained using the power quality analyzer HIOKI 3196.

B. Disturbance Rejection Performance and Transient Response

Another test has been performed with a sudden change in the active power in order to investigate the disturbance rejection performance and the dynamic response of the ADRC controller after step changes in the current reference. Fig. 18(a) and (b) show the step-up response and the step-down response of the grid-phase current when the d-axis grid current reference changes from 5 to 10 A and from 10 to 5 A, respectively. As expected, the grid current references are well tracked and the proposed control approach provides good dynamic performance with fast transient response and without overshoot. These results demonstrate also the strong disturbance rejection capability of the ADRC controller under sudden abrupt change of the active power.

C. Adaptability for Grid Environment

Finally, the robustness against parameters uncertainties has been further tested after variation of the grid-side inductance by 50% (from 100% to 150%). The grid-phase currents using the proposed ADRC control strategy are shown in Fig. 19. As can be seen, based on the proposed ADRC control method, the system still behaves stable enough. In contrast, the results with the classical notch-filter-based control method presented in Fig. 20 clearly show that the grid-phase currents are highly distorted; moreover, the oscillations present on the current waveforms imply that the control system is not stable due to the LCL-filter resonance. Thus, the inverter equipped with the proposed ADRC control strategy has a better adaptability for grid environment variations that confirms the results that have been achieved in simulations.

VI. CONCLUSION

Current controller design is a fundamental issue in the LCL-filter-based grid-connected VSI due to the LCL-filter resonance behavior, particularly when the system uncertainties and disturbances are considered. In this paper, robust current control is designed based on the LADRC. The mathematic model of the LCL-filtered grid-connected inverter system was analyzed and the low-order approximate model was acquired to simplify the control design. Simulation results show that the proposed current controller can ensure fast transient response and good steady-state performance even under parameters uncertainties and disturbances. Moreover, the current-controlled grid-connected converter with the LCL filter has good adaptability to grid environment imposed by the ADRC control, which is independent of the system model. Experimental results are also presented in order to validate the performance of the proposed controller in a real prototype. This paper is expected to provide more ideas for the engineers to apply the ADRC in power electronic converters control.

REFERENCES

[1] F. Blaabjerg, R. Teodorescu, M. Liserre, and A. Timbus, "Overview of control and grid synchronization for distributed power generation systems," *IEEE Trans. Ind. Electron.*, vol. 53, no. 5, pp. 1398–1409, Oct. 2006.

[2] M. Liserre, F. Blaabjerg, and S. Hansen, "Design and control of an LCL-filter-based three-phase active rectifiers," *IEEE Trans. Ind. Appl.*, vol. 41, no. 5, pp. 1281–1291, Sep./Oct. 2005.

[3] W. Wu, Y. Liu, Y. He, H. S. Chung, M. Liserre, and F. Blaabjerg, "Damping methods for resonances caused by LCL-filter-based current-controlled grid-tied power inverters: An overview," *IEEE Trans. Ind. Electron.*, vol. 64, no. 9, pp. 7402–7413, Sep. 2017.

[4] R. Peña-Alzola, M. Liserre, F. Blaabjerg, R. Sebastián, J. Dannehl, and F. W. Fuchs, "Analysis of the passive damping losses in LCL-filterbased grid converters," *IEEE Trans. Power Electron.*, vol. 28, no. 6, pp. 2642–2646, Jun. 2013.

[5] X. Wang, F. Blaabjerg, and P. C. Loh, "High-performance feedback-type active damping of LCL-filtered voltage source converters," in *Proc. IEEE Energy Convers. Congr. Expo.*, 2015, pp. 2629–2636.

[6] X. Wang, F. Blaabjerg, and P. Loh, "Grid-current-feedback active damping for LCL resonance in grid-connected voltage source converters," *IEEE Trans. Power Electron.*, vol. 31, no. 1, pp. 213–223, Jan. 2016.

[7] J. Dannehl, M. Liserre, and F. W. Fuchs, "Filter-based active damping of voltage source converters with LCL filters," *IEEE Trans. Ind. Electron.*, vol. 58, no. 8, pp. 3623–3633, Aug. 2011.

[8] W. Yao, Y. Yang, X. Zhang, F. blaabjerg, and P. C. Loh, "Design and analysis of robust active damping for LCL filters using digital notch filters," *IEEE Trans. Power Electron.*, vol. 32, no. 3, pp. 2360–2375, Mar. 2017.

[9] J. R. Massing, M. Stefanello, H. A. Grundling, and H. Pinheiro, "Adaptive current control for grid-connected converters with LCL filter," *IEEE Trans. Ind. Electron.*, vol. 59, no. 12, pp. 4681–4693, Dec. 2012.

[10] D. Pan, X. Ruan, C. Bao, W. Li, and X. Wang, "Capacitor-current feedback active damping with reduced computation delay for improving robustness of LCL-Type grid-connected inverter," *IEEE Trans. Power Electron.*, vol. 29, no. 7, pp. 3414–3427, Jul. 2014.

[11] Y. A.-R. I. Mohamed, M. A. Rahman, and R. Seethapathy, "Robust line-voltage sensorless control and synchronization of LCL-filtered distributed generation inverters for high power quality grid connection," *IEEE Trans. Power Electron.*, vol. 27, no. 1, pp. 87–98, Jan. 2012.

[12] K. Nishida, T. Ahmed, and M. Nakaoka, "Cost-effective deadbeat current control for wind-energy inverter application with LCL filter," *IEEE Trans. Ind. Appl.*, vol. 50, no. 2, pp. 1185–1197, Mar./Apr. 2014.

[13] A. Benrabah, D. Xu, and Z. Gao, "Uncertainty and disturbance estimator based current control of LCL-Filtered grid-connected inverters," Presented at the 2017 IEEE ITEC Asia-Pacific, Harbin, China, 2017.

[14] J. Han, "From PID to active disturbance rejection control," *IEEE Trans. Ind. Electron.*, vol. 56, no. 3, pp. 900–906, Mar. 2009.

[15] Y. Huang and W. Xue, "Active disturbance rejection control: Methodology and theoretical analysis," *ISA Trans.*, vol. 53, no. 4, pp. 963–976, 2014.

[16] Z. Gao, "Scaling and bandwidth-parameterization based controller tuning," in *Proc. Amer. Control Conf.*, 2003, pp. 4989–4996.

[17] C. Zhao and D. Li, "Control design for the SISO system with the unknown order and the unknown relative degree," *ISA Trans.*, vol. 53, no. 4, pp. 858–872, Jul. 2014.

[18] W. Xue, R. Madonski, K. Lakomy, Z. Gao, and Y. Huang, "Add-on module of active disturbance rejection for set-point tracking of motion control systems," *IEEE Trans. Ind. Appl.*, vol. 53, no. 4, pp. 4028–4040, Jul./Aug. 2017.

[19] W. C. Xue, W. Y. Bai, S. Yang, K. Song, Y. Huang, and H. Xie, "ADRC with adaptive extended state observer and its application to air-fuel ratio control in gasoline engines," *IEEE Trans. Ind. Electron.*, vol. 62, no. 9, pp. 5847–5857, Sep. 2015.

[20] Y. Q. Xia and M. Y. Fu, *Compound Control Methodology for Flight Vehicles*. Berlin, Germany: Springer-Verlag, 2013.

[21] A. Benrabah, D. Xu, X. Wang, and F. Blaabjerg, "Robust active damping control of LCL filtered grid connected converter based active disturbance rejection control," in *Proc. IEEE Energy Convers. Congr. Expo.*, 2016, pp. 2661–2666.

[22] X. Wang, F. Blaabjerg, Z. Chen, and W. Wu, "Resonance analysis in parallel voltage-controlled distributed generation inverters," in *Proc. IEEE Appl. Power Electron. Conf. Expo.*, 2013, pp. 2977–2983.

[23] F. Wang, J. Duarte, M. Hendrix, and P. Ribeiro, "Modelling and analysis of grid harmonic distortion impact of aggregated DG inverters," *IEEE Trans. Power Electron.*, vol. 26, no. 3, pp. 786–797, Mar. 2011.

[24] A. Benrabah, D. Xu, and Z. Gao, "Active disturbance rejection control of *LCL* filtered grid-connected inverter using Padé approximation," Presented at the 2017 IEEE ITEC Asia-Pacific, Harbin, China, 2017.

[25] R. Pena-Alzola, M. Liserre, F. Blaabjerg, M. Ordonez, and Y. Yang, "*LCL*-filter design for robust active damping in grid connected converters," *IEEE Trans. Ind. Informat.*, vol. 10, no. 4, pp. 2192–2203, Nov. 2014.

[26] W. Yang, W. Cao, T. Chung, and J. Morris, *Applied Numerical Methods Using Matlab*. Hoboken, NJ, USA: Wiley, 2005.

[27] T. Yi, L. Poh Chiang, W. Peng, C. Fook Hoong, and G. Feng, "Exploring inherent damping characteristic of *LCL*-filters for three-phase gridconnected voltage source inverters," *IEEE Trans. Power Electron.*, vol. 27, no. 3, pp. 1433–1443, Mar. 2012.

[28] Y. Xia, P. Shi, G. Liu, D. Rees, and J. Han, "Active disturbance rejection control for uncertain multivariable systems with time-delay," *IET Control Theory Appl.*, vol. 1, pp. 75–81, 2007.

[29] S. Zhao and Z. Gao, "Modified active disturbance rejection control for time-delay systems," *ISA Trans.*, vol. 53, no. 4, pp. 882–888, Jul. 2014.

[30] Q. Zheng, L. Gao, and Z. Gao, "On stability analysis of active disturbance rejection control for nonlinear time-varying plants with unknown dynamics," in *Proc. IEEE Conf. Decis. Control*, 2007, pp. 12–14.

[31] G. Herbst, "Practical active disturbance rejection control: Bumpless transfer, rate limitation, and incremental algorithm," *IEEE Trans. Ind. Electron.*, vol. 63, no. 3, pp. 1754–1762, Mar. 2016.

[32] Q. Zheng, Z. Chen, and Z. Gao, "A dynamic decoupling control approach and its applications to chemical processes," in *Proc. Amer. Control Conf.*, 2007, pp. 5176–5181.

[33] M. Przybyła, M. Kordasz, R. Madoński, P. Herman, and P. Sauer, "Active disturbance rejection control of a 2DOF manipulator with significant modeling uncertainty," *Bull. Polish Acad. Sci., Tech. Sci.*, vol. 60, pp. 509–520, 2012.

[34] S. Luo *et al.*, "On decoupling trajectory tracking control of unmanned powered parafoil using ADRC-based coupling analysis and dynamic feedforward compensation," *Nonlinear Dyn.*, vol. 92, pp. 1619–1635, 2018.

Abdeldjabar Benrabah was born in Skikda, Algeria, in 1988. He received the Engineering degree in electrical engineering from Polytechnic Military School, Algiers, Algeria, in 2012. He is currently working toward the Ph.D. degree at Harbin Institute of Technology, Harbin, China.

His research interests include control of grid connected converters, renewable energy, and microgrids.

Dr. Benrabah was recipient of the Chinese Government Outstanding International Student Scholarship in 2017.

Dianguo Xu (M'97–SM'12–F'17) was born in Heilongjiang, China, in 1960. He received the B.S. degree in control engineering from Harbin Engineering University, Harbin, China, in 1982, and the M.S. and Ph.D. degrees in electrical engineering from Harbin Institute of Technology (HIT), Harbin, China, in 1984 and 1989, respectively.

In 1984, he was an Assistant Professor with the Department of Electrical Engineering, HIT, where he has been a Professor, since 1994. He was the Dean of School of Electrical Engineering and Automation, HIT, from 2000 to 2010. He is currently the Vice President with HIT. His research interests include renewable energy generation technology, power quality mitigation, sensorless vector-controlled motor drives, high-performance servo system. He authored or coauthored more than 600 technical papers.

Dr. Xu is an Associate Editor for the IEEE TRANSACTIONS ON INDUSTRIAL ELECTRONICS, the IEEE TRANSACTIONS ON POWER ELECTRONICS, and the IEEE JOURNAL OF EMERGING AND SELECTED TOPICS IN POWER ELECTRONICS. He is the Chairman of the IEEE Harbin Section.
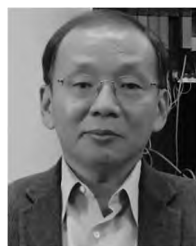
Zhiqiang Gao received the Ph.D. degree in electrical engineering from the University of Notre Dame, Notre Dame, IN, USA, in 1990.

He is an Associate Professor and the Director of the Center for Advanced Control Technologies, Cleveland State University, Cleveland, OH, USA. His research interests include principles and practice of engineering cybernetics, particularly its manifestation in active disturbance rejection control.